Solid polymer electrolytes based on lithium bis(trifluoromethanesulfonyl)imide/poly(vinylidene fluoride -co-hexafluoropropylene) for safer rechargeable lithium-ion batteries

R. Gonçalves[1,2#], D. Miranda[3,#], A. M. Almeida[1], M.M. Silva[4], J. M. Meseguer-Dueñas[5,6], J. L. Gomez Ribelles[5,6], S. Lanceros-Méndez[7,8], C. M. Costa[1,4]

[1]Centro de Física, Universidade do Minho, 4710-057 Braga, Portugal

[2]Institute of Science and Innovation for Bio-Sustainability (IB-S), University of Minho, Portugal

[3]2Ai- Instituto Politécnico do Cávado e Ave, Barcelos, Portugal

[4]Centro de Química, Universidade do Minho, 4710-057 Braga, Portugal

[5]Centre for Biomaterials and Tissue Engineering, CBIT, Universitat Politècnica de València, 46022 Valencia, Spain

[6]Biomedical Research Networking Center on Bioengineering, Biomaterials and Nanomedicine (CIBER-BBN), Valencia, Spain

[7]BCMaterials, Basque Center for Materials, Applications and Nanostructures, UPV/EHU Science Park, 48940 Leioa, Spain.

[8]IKERBASQUE, Basque Foundation for Science, 48013 Bilbao, Spain

[#]equal contribution

Abstract:

The increasing use of electronic portable systems and the consequent energy demand, leads to the need to improve energy storage systems. According to that and due to safety issues, high-performance non-flammable electrolytes and solid polymer electrolytes (SPE) are needed.

SPE containing different amounts of lithium bis(trifluoromethanesulfonyl)imide (LiTFSI) into a poly(vinylidene fluoride-co-hexafluoropropylene), PVDF-HFP, polymer matrix have been prepared by solvent casting. The addition of LiTFSI into

PVDF-HFP allows to tailor thermal, mechanical and electrical properties of the composite.

In particular, the ionic conductivity of the composites increases with LiTFSI content, the best ionic conductivities of 0.0011 mS/cm at 25º C and 0.23 mS/cm at 90 ºC were obtained for the PVDF-HFP/LiTFSI composites with 80wt.% of LiTFSI.

This solid electrolyte allows the fabrication of Li metallic/SPE/C-$LiFePO_4$ half-cells with a discharge capacity of 51.2 $mAh.g^{-1}$ at C/20. Further, theoretical simulations show that the discharge capacity value depends on the lithium concentration and percentage of free ions and is independent of the solid polymer electrolyte thickness. On the other hand, the voltage plateau depends on the SPE thickness. Thus, a solid electrolyte is presented for the next generation of safer solid-state batteries.

Keywords: solid polymer electrolyte; PVDF-HFP; LiTFSI; composites; simulations; Li-ion batteries

1. Introduction

The present highly technological and energy dependent society continuously demands efficient energy storage devices with higher energy density and safety for portable consumer devices and electric vehicles, lithium-ion batteries playing an increasing role [1, 2]. Rechargeable lithium-ion batteries still show the highest energy density when compared to other battery systems, such as NiCd (nickel-cadmium) and NiMH (nickel-metal hydride), and dominate the global market for energy storage systems [3].

To improve Li-ion battery energy density and safety, further developments are needed at the levels of its components: electrodes and separator/electrolyte [4, 5]. A relevant and major issue that requires special attention is the safety of the batteries, with the separator/electrolyte playing an essential role [6].

There are several types of electrolytes but the most used are still the liquid electrolytes with different lithium salts types. Those electrolytes are generally based on organic alkyl carbonates that are volatile and flammable, and therefore, represent a problem

with respect to battery safety [7]. Another problem of the liquid electrolytes is its reaction with lithium metal that results in the growth of Li dendrites which render internal short circuits that often lead to overheating and ignition, causing battery explosion [8].

In order to solve these safety problems, the use of non-flammable electrolytes without organic alkyl carbonates and solid polymer electrolytes (SPE) have been intensively studied, considered as suitable candidates [9] for solid-state rechargeable batteries [10].

SPEs mostly consist of dissolved lithium salts in a polymer matrix [11]. In addition to the lithium salts, different nanofillers, such as ceramic or metals, can be also added to improve the mechanical and electrochemical properties [12]. A polymer matrix that stands out due to its exceptional properties and characteristics, including high polarity, excellent thermal and mechanical properties, being chemically inert and stable in cathodic environment, is poly(vinylidene fluoride) (PVDF) and its copolymers PVDF-co-trifluoroethylene (PVDF-TrFE) and PVDF-co-hexafluoropropene (PVDF-HFP) [13]. When compared to the others PVDF copolymers, PVDF-HFP is an excellent polymer matrix for SPEs due to its low degree of crystallinity, which allows improving ionic conductivity. It also shows excellent mechanical properties and high dielectric constant (~7 to 9), as well as highly polar functional groups (-C-F) [14].

In relation to lithium salts, lithium bis(trifluoromethanesulfonyl)imide (LiTFSI) is widely used in SPE development, considering its excellent electrochemical properties, high chemical and thermal stability and because its large and bulky anions can be highly delocalized to facilitate the salt dissociation and solubility [15, 16].

The literature reports some works on SPEs based on PVDF-HFP and LiTFSI based on different approaches with respect to the preparation conditions [17] as well as with respect to the addition of different fillers (1-ethyl-3-methylimidazolium bis(trifluoromethanesulfonyl)imide (EMITFSI) [18], silica [19], lithium aluminum titanium phosphate (LATP) [20], nickel-1,3,5-benzene tricarboxylate metal organic framework (Ni_3-$(BTC)_2$-MOF) [21], and 1-cyanomethyl-3-methylimidazolium bis(trifluoromethylsulfonyl)imide ($[CCNIm^+][TFSI^-]$) [22]. For these SPE, the ionic conductivity value is between 10^{-5} $S.cm^{-1}$ and 0.25 $mS.cm^{-1}$, but electrical properties, thermal and mechanical stability, must still be improved.

Polymer gel electrolytes (PGEs) have been prepared by dissolving LiTFSI in 1-methyl-3-propylpyrrolidinium bis(trifluoromethanesulfonyl)imide (P_{13}TFSI) ionic liquid mixing the electrolyte solution with PVDF-HFP copolymer. Further, small amounts of

ethylene carbonate were added to the PGEs in order to improve the ionic conductivity and Li ion transport kinetics of the electrolytes [23].

Adding propylene carbonate (PC) contents up to 30wt% into the SPE acts as plasticizer and improves ionic conductivity. Thus, SPEs based on PVDF-HFP and LiTFSI and PC with solid-like mechanical stability presents a high conductivity of 1×10^{-5} S.cm^{-1} at the composition 0.55/0.15/0.30 wt% PVdF-HFP/LiTFSI/PC [17]. Another SPE based on different materials are (PVDF-HFP with $Li_7La_3Zr_2O_{12}$ [24], (PEO)-$LiClO_4$-$Li_{1.3}Al_{0.3}Ti_{1.7}(PO_4)_3$ (LATP)) [25] and PEO-MIL-53(Al)-LiTFSI [26] which have been prepared for different types of solid-state batteries, including sodium-ion [27], Al batteries based on NASICON materials [28] and lithium-vanadium batteries [26].

In SPE ions may be present either as free ions, contact ion pairs or diffusion ion pairs, the ionic conductivity value being essential for obtaining high capacity in the battery [29]. In solid state batteries it is essential to improve the ionic conductivity of the SPEs, at room and/or battery operation temperature, and consequently battery performance [30]. This can be only achieved through proper understating of the interactions between ions and polymeric matrix and the contribution of ions to the electrical response.

Based on the literature and maintaining a fixed PC content, the goal of this work is to prepare and optimize SPE based on PVDF-HFP polymer and high amounts of LiTFSI salt. Samples were prepared by solvent casting with different LiTFSI contents up to 80wt.%. The influence of LiTFSI content in the microstructure, ion-polymer interaction, ionic conductivity of the SPE, and charge-discharge performance of the SPE in the cathodic C-$LiFePO_4$ half-cells were evaluated.

Also, the charge-discharge behavior and cycling performance of the SPE are correlated with the theoretical 1D model simulation of Li-ion Solid State Batteries (SSB) in order to properly understand and optimize its performance.

The theoretical simulations were performed as a function of lithium concentration, percentage of free ions and solid polymer electrolyte thickness.

2. Experimental details

2.1. Materials

Poly(vinylidene fluoride-co-hexafluropropylene), PVDF-HFP, Solef 21216 (M_w = 600.000 Da, VDF/HFP mole ratio equal to 88/12) and lithium bis (trifluoromethanesulfonyl) imide (LiTFSI) were acquired from Solvay and Solvionic,

respectively. Propylene carbonate (PC, anhydrous 99.0%) and *N*,*N*-dimethylformamide (DMF) were purchased from Sigma-Aldrich and Merck, respectively.

2.2. **Solid polymer electrolyte preparation**

PVDF-HFP/LiTFSI composites were prepared after the protocol presented in [31] by dissolving the appropriate amounts of LiTFSI at a 10/90 w/v polymer/solvent ratio. The solvent ratio is 75 v.% of DMF and 25v.% of PC. This composition was selected in order to obtain good dissolution of high amounts of LiTFSI up to 80wt.%.

First, the LiTFSI salts were added to the solvents. After complete dissolution of the salts, the polymer was added to the solution at 25 ºC and stirred for 4 hours until a homogeneous and transparent solution was obtained.

The solution was spread on a clean glass substrate by blade coating and placed in an oven at 210 ºC for 15 minutes to ensure solvent evaporation and polymer melting.

After cooling to room temperature, PVDF-HFP/LiTFSI composites with average thickness of ~ 100 μm were obtained and will be identified henceforth by the LiTFSI content.

2.3. **Characterization techniques**

2.3.1. Morphological and physicochemical characterization of the PVDF-HFP/LiTFSI composites

The microstructure of the PVDF-HFP/LiTFSI composites was analyzed by scanning electron microscopy (SEM, Cambridge, Leica) with an accelerating voltage of 3 kV. The samples were previously coated with a thin gold layer using a sputter coating (Polaron, model SC502 sputter coater).

Polymer phase and ion-polymer interaction in the PVDF-HFP/LiTFSI composites were investigated at room temperature by Fourier Transformed Infrared (FTIR) spectroscopy in the ATR mode from 4000 to 600 cm^{-1} after 64 scans with a resolution of 4 cm^{-1} using a Jasco FT/IR-4100.

Thermogravimetric Analysis (TGA) was performed using a Q600 TGA TA thermobalance operating between 40 and 800 °C. The PVDF-HFP/LiTFSI composites were placed in open ceramic crucibles, α-Al_2O_3 pans, with a sample weight of ~10 mg,

and measured at a heating rate of 10 °C/min under a nitrogen atmosphere flow of 50 mL/min.

Differential scanning calorimetry analysis (DSC) was carried out with a Perkin-Elmer DSC 8000 instrument under a flowing nitrogen atmosphere between -90 and 150 °C at a heating rate of 20 $^{o}C.min^{-1}$. All samples were measured in 30 µL aluminium pans with perforated lids to allow the release and removal of decomposition products.

Mechanical tests were performed with a universal testing machine (Shimadzu model AG-IS) at room temperature with a load cell of 50 N in the tensile mode. The stress-strain characteristic curves were obtained until rupture in samples with typical dimensions of 10×4×0.100 mm at 0.5 mm/min.

2.3.2. Electrochemical properties and lithium half-cell preparation and testing

The ionic conductivity of the PVDF-HFP/LiTFSI composites was measured by impedance spectroscopy in an Autolab PGSTAT-12 (Eco Chemie) at frequencies between 500 mHz and 65 kHz in the temperature range from 20 to 90 ^{o}C, using a constant volume support equipped with gold blocking electrodes placed within a Buchi TO 50 oven. The sample temperature was evaluated by means of a type K thermocouple placed close to the composite.

The ionic conductivity (σ_i) was calculated according to equation 1:

$$\sigma_i = \frac{d}{R_{b.}A} \quad (1)$$

where R_b represents the sample bulk resistance, obtained by impedance spectroscopy, d is the thickness of the sample and A is the electrochemical active area, respectively.

Composite cathode electrodes were prepared by mixing the active material (C-$LiFePO_4$), conductive active (Super-P C45) and the PVDF binder in N-methyl-pyrrolidone, NMP, with relation 80/10/10 wt.%, respectively. More details on the cathode electrode preparation can be found in [32].

Li/C-$LiFePO_4$ half-cells were assembled in an argon-filled glove box (H_2O, O_2 < 1ppm) using Swagelok-type cells with C-$LiFePO_4$ electrode (8 mm diameter) as working electrode, PVDF-HFP/LiTFSI composite (10 mm diameter) as solid polymer electrolyte and 1.5 mm thick Li metal foil (8 mm diameter) as reference/counter electrode

The cycling performance of the Li/C-$LiFePO_4$ half-cells was investigated in galvanostatic mode within the 2.5-4.2 V voltage range at C/20 rate (C=170 $mAh.g^{-1}$) at room temperature using a Landt CT2001A instrument.

3. Theoretical simulation model and parameters

3.1.Theoretical simulation model

The theoretical simulations were performed in order to predict the performance of the solid-state lithium ion batteries when subjected to variations of the electrochemical and geometric variables of the separator component, such as, concentration of lithium, free lithium ions concentration and separator thickness. Further, battery performance was evaluated at different discharge rates to account for variations in the energy efficiencies [33].

The simulations were carried out by implementing the finite element method in MATLAB scripts in order to solve the equations describing the behaviour of battery electrodes and separator (table 1) for the following solid-state lithium-ion battery structure: [negative electrode, lithium foil | solid polymer electrolyte, separator | positive electrode, (Li_xFePO_4)]. The batteries were implemented in half-cells and represented by a 1D model, as shown in figure 1.

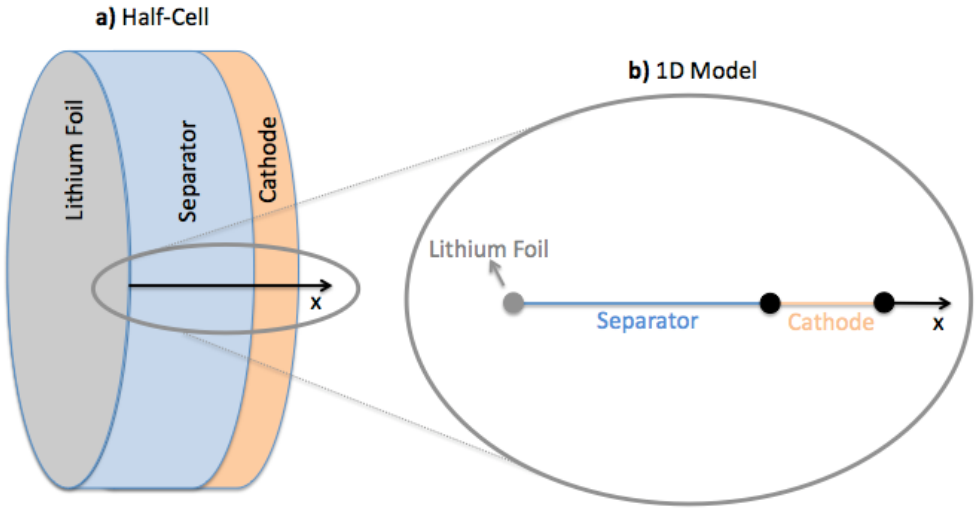

Figure 1 – Schematic representation of: **a)** solid-state lithium-ion half-cell **b)** representation of the half-cell in the theoretical model (1D model).

Within the half-cells it was considered the solid polymer electrolyte as the separator and the positive electrode (cathode). The simulations are time-dependent and the

electrochemical model describes the electrochemical and physical processes that occur in the operation of solid state lithium batteries, such as, electrochemical reactions, lithium ion diffusion, electron and solid lithium transport [34].

The fundamental equations governing the main phenomena of the operation processes of lithium ion solid-state micro-batteries are based on the Danilov et al. [35] model in 1D and the A. Bates et al. [34] model for 2D. The electrochemical model describes the migration and diffusion of lithium ions through the solid electrolyte using the Nernst–Plank equation and the solid lithium transport in the positive electrode was calculated using the Fick's law. The reaction kinetics that occurs in both electrode/electrolyte interfaces were calculated by the Butler-Volmer equation.

The electrochemical model takes into account the variables corresponding to the phenomena occurring in the separator and the positive electrode, such as the electrolyte potential, the concentration of lithium ions in the electrolyte/separator, the concentration of solid lithium at the positive electrode, and the electric potential at the boundary interface between each electrodes (lithium foil and cathode) and separator. Table 1 shows the main equations governing the operation of the half-cell solid-state lithium-ion battery electrodes and separator.

Table 1 - Summary of the main equations governing solid-state lithium-ion half-cells [34-36]. The identification of each symbol is provided in the nomenclature section.

Electrochemical model (Solid-State Lithium ion half-cell)		
Physical process	**Governing Equation**	**Region**
Transport of Li^+ and n^- in the electrolyte (Nernst–Planck equation)	$N_i = -D_i.\nabla c_i + \left(\frac{z_i.F}{RT}\right) D.c_i.\nabla\phi_E, i = Li^+, n^-$	Separator
Transport of solid lithium through the positive electrolyte (Fick's law)	$N_{Li} = -D_{Li}.\nabla c_{Li}$	Electrodes
Fraction of total lithium dissociated at equilibrium	$c_{Li^+}^{Eq} = c_{n^-}^{Eq} = \delta c_0$	Separator
Overpotential	$\eta = \phi_0 - \phi_E - E_{eq,i}$	Electrodes
Lithium ion recombination	$r_{Li^+ = k_{diss}\left(c_{0,Li^+} - c_{Li^+}\right) - k_{rec}(c_{Li^+})c_{n^-}}$	Separator

/ dissociation rate		
Relation between the dissociation reaction rate (k_{diss}) and the recombination reaction rate (k_{rec})	$k_{diss} = \frac{k_{rec}.c_{0,Li^+}.\delta^2}{1-\delta}$	Separator
Reaction kinetics at the negative electrode (Butler-Volmer equation)	$i_{neg} = F.k_{neg}\left(\frac{c_{Li^+}}{C_{0,Li^+}}\right)^{\alpha_{neg}}\left(e^{\left(\alpha_{neg}Fn/RT\right)} + e^{-\left((1-\alpha_{neg})Fn/RT\right)}\right)$	Electrode / electrolyte interface
Reaction kinetics at the positive electrode (Butler–Volmer equation)	$i_c = i_{0,c}\left(e^{\alpha_c Fn/RT} + e^{-(1-\alpha_c)Fn/RT}\right)$ $i_{0,c} = Fk_c\left(\frac{(c_{Li,max}-c_{Li})c_{Li^+}}{(c_{Li,max}-c_{Li,min})c_{0,Li^+}}\right)^{\alpha_c}\left(\frac{c_{Li}-c_{Li,min}}{c_{Li,max}-c_{Li,min}}\right)1-\alpha_c$	Electrode / electrolyte interface

3.2. Specific parameters and initial values

The parameters and initial values used for the simulation of the solid-state lithium ion batteries are listed in Table 2.

Table 2 - Values of the parameter used in the simulations. The nomenclature is provided in the nomenclature section.

Electrochemical parameters and initial values			
Parameter	**Unit**	**Separator**	**Cathode** (Li_xFePO_4)
L_i	m	100×10^{-6}	20×10^{-6}
c_{0,Li^+}	mol/m^3	3483,23 [b] $\times$ δ	
δ	----------	0,20	
$c_{Li,max}$	mol/m^3		23300
$c_{Li,min}$	mol/m^3		10200
k_{rec}	m^3/mol.s	$0,9\times10^{-8}$ [a]	
D_{Li^+}	m^2/s	$0,9\times10^{-13}$ [a]	
D_{n^-}	m^2/s	$1,25\times10^{-13}$	

D_{Li}	m^2/s		$1,8\times10^{-15}$
α_c	----------		0,6 [a]
k_c	$mol/m^2.s^{-1}$		$5,1\times10^{-4}$ [a]
Negative Electrode (Lithium foil)			
α_{neg}	----------	0,5 [a]	
k_{neg}	$mol/m^2.s^{-1}$	1×10^{-2} [a]	
General parameters of battery			
i_{app}	A/m^2	6,10 [b]	
F	C/mol	96487	
R	J/mol.K	8,314	
T	K	298,15	

[a] Based on [34].

[b] Experimental value.

4. Results and discussions

4.1. Morphological and physicochemical characterization

4.1.1. Composites morphology

In order to evaluate the effect of LiTFSI salts on the morphology of the PVDF-HFP composites, SEM images are presented in Figure 2a-b first for the PVDF-HFP films without LiTFSI salts in both surface (a) and cross-section (b) views, revealing a compact structure without pores, which is attributed to the melting and recrystallization process during sample preparation [31, 37].

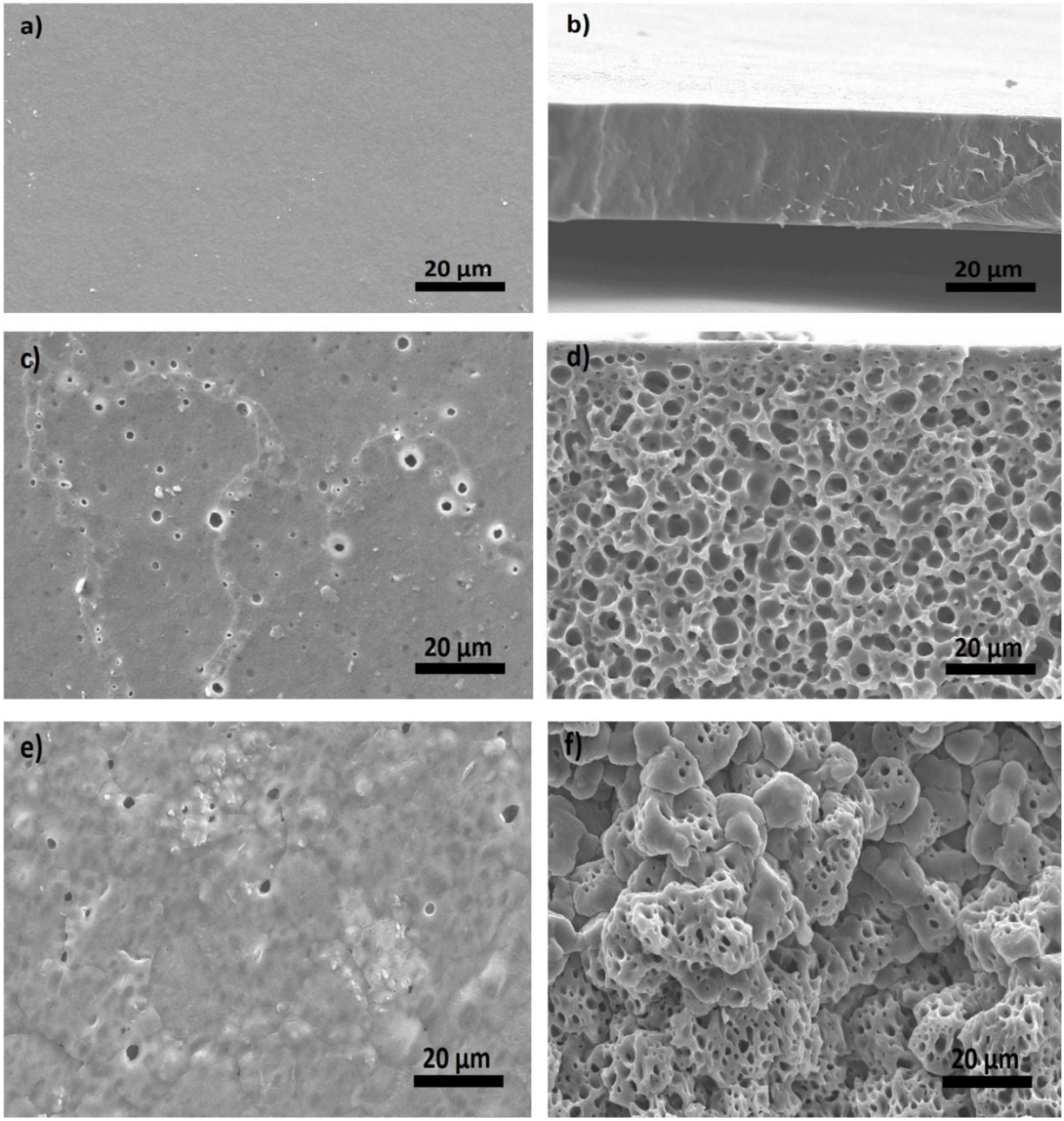

Figure 2 - Surface and cross-section SEM images for the PVDF-HFP/LiTFSI composites with different LiTFSI amounts: a-b) 0 wt.%, c-d) 50 wt.% and e-f) 80 wt.%.

When the LiTFSI salts are introduced into the PVDF-HFP matrix, a porous microstructure is observed regardless of the LiTFSI content, as verified in figures 2c-f. The porous microstructure is attributed to the free space between the LiTFSI salts (Figure 2c-f) and has been previously reported [18, 38]. In addition, it is observed that the pore distribution occurs homogeneously throughout the sample. Figure 2 shows that SEM images for LiTFSI contents of 50 wt.% (figure 2c-d) and 80 wt.% (figure 2f-e), but the porous microstructure is observed for all PVDF-HFP/LiTFSI composites. It is to

notice that this microstructure is highly desirable for solid electrolytes as it facilitates the conduction of the ions [38, 39].

4.1.2. Polymer phase, thermal and mechanical properties

ATR-FTIR spectra allows identifying the characteristic bands of PVDF-HFP polymer and LiTFSI salts, as well as new bands or band modifications related to ion-polymer interactions.

Figure 3a shows the ATR-FTIR spectra for the different PVDF-HFP/LiTFSI composites with the rectangles in different colors representing the main vibrational bands of PVDF-HFP [40]. The peaks at 760, 795, 974 and 1384 cm^{-1} correspond to α phase crystals (TGTG chain conformation) [37], and decrease with increasing LiTFSI content within the polymer. The vibration bands at 1064 and 1148 and cm^{-1} are assigned to the symmetrical stretching mode of CF_2 and the displacement of these broad peaks to the left indicate the strong interaction with LiTFSI. This fact is also confirmed by the bands in the region 1380 to 1420 cm^{-1} corresponding to the vibrations of the CH_2 group, which also show shape changes and intensity variations. Further, figure 3a) also show the vibrations peaks for LiTFSI at 842 and 1357 cm^{-1} that correspond to N-CO-O symmetric stretching and asymmetric SO_2 stretching modes, respectively [41, 42].

The thermal evaluation of the PVDF-HFP/LiTFSI composites was performed by TGA thermograms, which are shown in figure 3b for the different PVDF-HFP/LiTFSI composites. Figure 3b shows that the thermal decomposition of pristine PVDF-HFP occurs in a single step at ~465 ºC [43], whereas for PVDF-HFP/LiTFSI composites, a two steps decomposition is observed: the first decomposition at ~ 340 ºC is related to the degradation temperature of LiTFSI [44] and the second one is related to the degradation of the polymer. For PVDF-HFP/LiTFSI composites with LiTFSI above 30% a small loss of weight is observed after 100 °C related to the moisture that can be absorbed during the handling of the test sample. Figure 3b) confirms that all PVDF-HFP/LiTFSI composites are thermally stable up to 100 °C, confirming their suitability for lithium-ion battery applications.

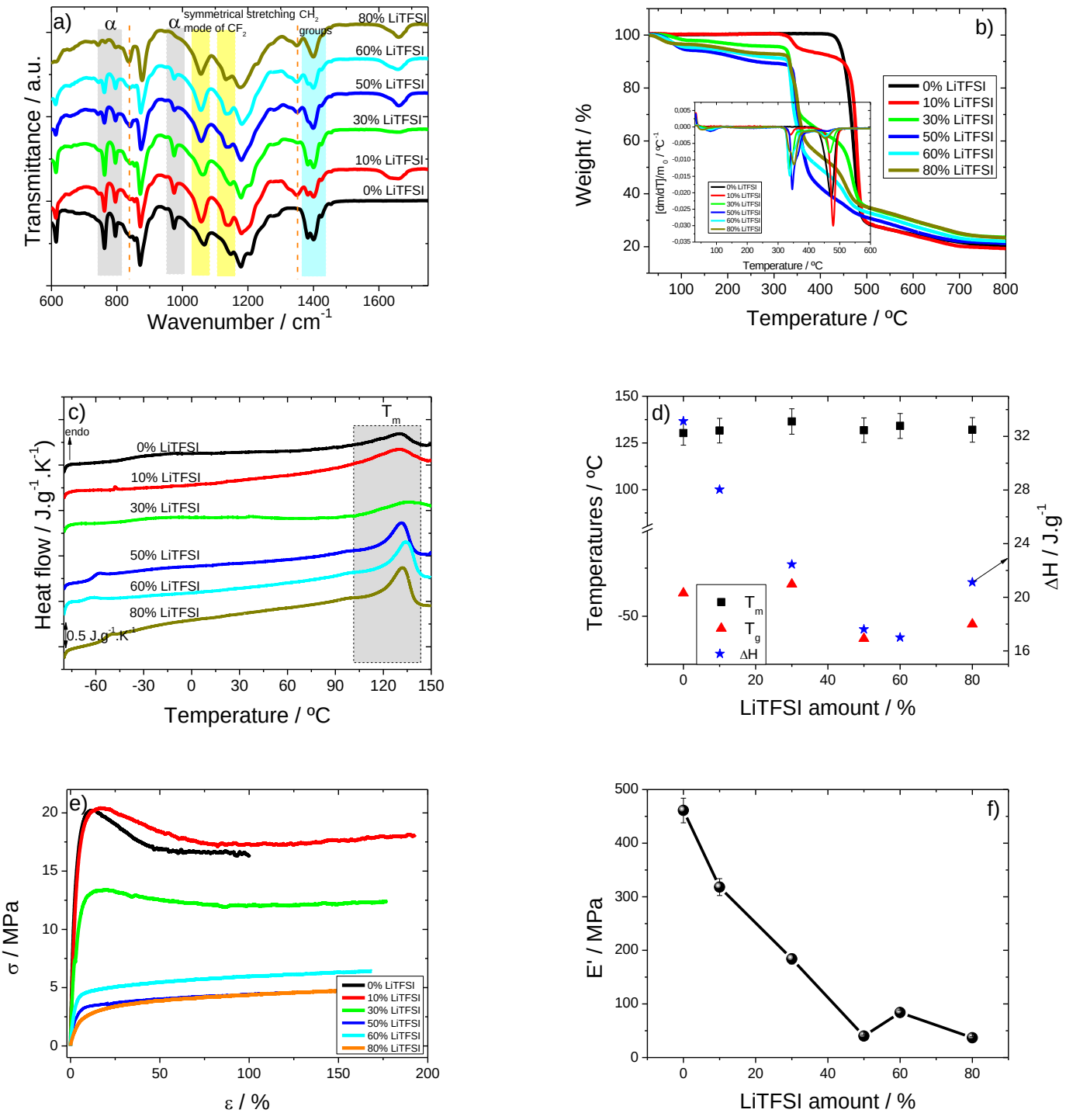

Figure 3 – a) ATR-FTIR spectra, b) TGA thermogram, c) DSC curves and e) Stress-Strain results for PVDF-HFP/LiTFSI composites. d) Melting (T_m) and glass (T_g) transition temperatures and melting enthalpy (ΔH) determined from the DSC curves and f) Young modulus as a function of the LiTFSI content.

The DSC thermograms of the PVDF-HFP/LiTFSI composites with the melting and glass temperature and melting enthalpy as a function of LiTFSI content are shown in

figures 3c and 3d, respectively. Regardless of the LiTFSI content, the melting behavior is similar and characterized by a melting peak around T_m ~130 ºC, as in pristine PVDF-HFP [40] (figure 3d). On the other hand, the glass transition temperature (T_g) as a function of LiTFSI content, figure 3d, shows that T_g decreases with increasing LiTFSI content, which shows strong intermolecular interaction between salts and polymer which significantly improve the segmental movement of the polymer network, leading to a more flexible polymer matrix [44]. Figure 3d also shows the melting enthalpy value as a function of the LiTFSI amount. The enthalpy is calculated by the area in the melting peak and is related to the degree of crystallinity of the polymer. It is observed that the enthalpy value and consequently the degree of crystallinity of PVDF-HFP copolymer decreases with the addition of LiTFSI in the PVDF-HFP polymer due to the complexation with LiTFSI salts (figure 3d).

Suitable mechanical properties of the PVDF-HFP/LiTFSI composites are essential for lithium-ion battery applications [45]. Figure 3e) shows the stress-strain characteristics curves of the PVDF-HFP/LiTFSI as well as the corresponding Young modulus, calculated at 3% in the elastic region, as a function of the LiTFSI content (figure 3f). All PVDF-HFP/LiTFSI composites show the typical mechanical behavior of thermoplastics, characterized by two regions (elastic and plastic), separated by the yielding region. The maximum elongation of all PVDF-HFP/LiTFSI composites is practically the same, independently of the LiTFSI content, with the exception of the pristine PVDF-HFP. The yielding stress (figure 3e) and the Young modulus (figure 3f), determined at 3% of maximum elongation in the elastic region by the tangent method [46], decrease with increasing LiTFSI content. These facts are consistent with a significant drop in the degree of crystallinity of the polymer as observed by the DSC curves (figure 3c-d). In any case, the stress-strain curves confirm the suitable mechanical properties of the composites for battery applications, even for the highest LiTFSI contents.

4.2. Ionic conductivity

The ionic conductivity was evaluated by impedance spectroscopy in the temperature range from 25 ºC to 90 ºC and the frequency range from 10 Hz to 10 MHz.

Figure 4a shows the Nyquist plot for the PVDF-HFP/LiTFSI composites at 25 ºC. Typically, the Nyquist plot represented in figure 4a, shows three characteristics parts as shown for the PVDF-HFP/LiTFSI composites with 0 and 50 wt% LiTFSI: a semicircle located in the high-frequency range that corresponds to the charge transfer process (bulk material properties), a transition controlled by the diffusion of counter ions inside the electrode, and straight line for lower frequency that is related to the diffusion process, i.e. the sample/electrode interface [47, 48]. It is to notice that in the insert of figure 4a for 80 wt.% LiTFSI, the semicircle is not observed due to the higher amount of lithium salts for this sample.

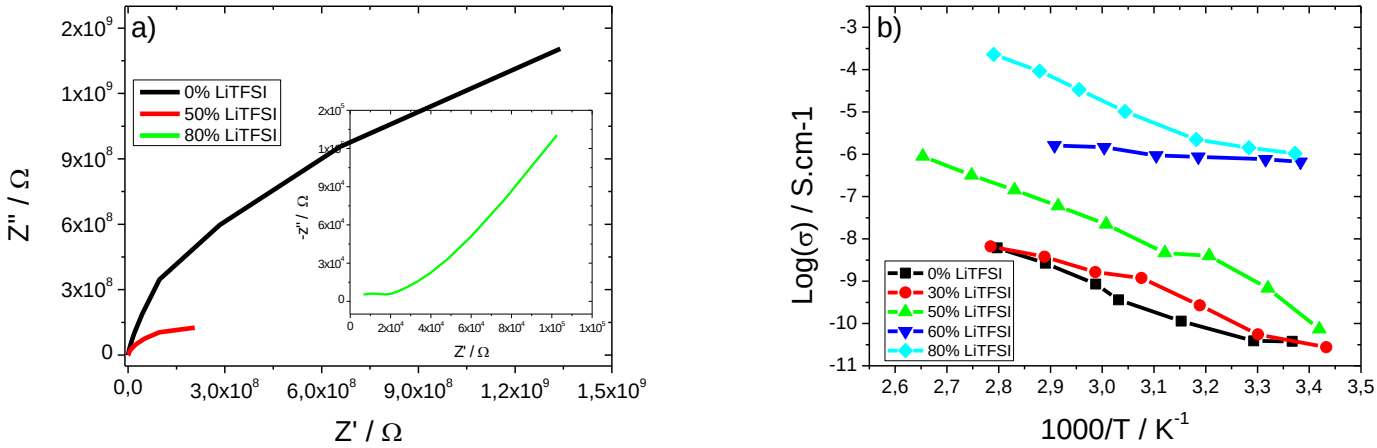

Figure 4 – a) Nyquist plots and b) logarithm of conductivity, σ, as a function of reciprocal temperature, 1000/T, for the PVDF-HFP/LiTFSI composites

At 25 ºC, the radius of the semicircle depicted in figure 4a (the ionic resistance being calculated in the Z' axis interception) decreases as the amount of LiTFSI increases. Increasing LiTFSI content reduces the bulk resistance by increasing the number of free charge carriers.

The temperature dependent ionic conductivity (calculated through equation 1) of the PVDF-HFP/LiTFSI composites is shown in figure 4b. Independently of the LiTFSI content, figure 4b shows that the ionic conductivity increases with increasing temperature due to the increase of the free volume, polymer segmental mobility and charge mobility [49]. For a given temperature, the ionic conductivity value increases with increasing LiTFSI content, as previously mentioned, due to enhanced charge carrier density [50]. A maximum ionic conductivity value of 0.0011 mS/cm at 25 ºC is obtained for the PVDF-HFP/LITFSI composites with 80 wt.% filler content. For this

same sample at 90 ºC, the ionic conductivity is 0.23 mS/cm, the temperature dependence of the ionic conductivity of PVDF-HFP/LiTFSI composites being ruled by a thermally activated process that can be adjusted by the Arrhenius equation to calculate the apparent activation energy for ion transport [51]. In this context, the activation energy for the PVDF-HFP/LITFSI composites with 80 wt.% is 0.36 eV.

The solid polymer electrolyte acts as a separator within the battery, providing a medium for ion transport between the electrodes. Thus, the PVDF-HFP/LiTFSI composite with the best ionic conductivity is the one with 80 wt.% LiTFSI.

4.3. Cycling performance

For actual battery applications, the cycling performance was evaluated at room temperature for the sample with 80 wt.% LiTFSI.

It is to notice that, comparing the results on the present battery with the ones from the literature, that typically, battery performance of solid-state batteries is evaluated at high temperatures (table 3) which limits their applicability.

Table 3 – Some examples of SPE cycled at high temperatures.

Polymer	**Salts**	**σi / mS.cm^{-1}**	**Capacity / mAh.g^{-1}**	**Temp / ºC**	**Ref**
TPU/PEO	LiTFSI	0.54	140@0.2C	60	[30]
PEO	LiTFSI	0.0054	168@0.2C	80	[52]
PEG	LiTFSI	0.19	----	60	[53]
PEG	LiTFSI	----	123@1C	60	[54]
P(LA-co-TMC)	LiTFSI	0.47	46@1C	55	[55]
PEO	LiTFSI	0.0045	122@1C	80	[56]

In order to evaluate the suitability of the developed solid electrolyte for battery applications, cathodic half-cells were fabricated and the cycling performance evaluated at a low scan rate of C/20 at room temperature due to its ionic conductivity value. Further, the influence of solid polymer electrolyte thickness and ions concentration were evaluated by theoretical simulation.

4.3.1. Experimental results

Charge-discharge voltage profiles of the Li/C-$LiFePO_4$ half-cells with the PVDF-HFP/LiTFSI composite with 80 wt.% and 100 µm of thickness as SPEs were recorded at a rate of C/20 between 2.5 and 4.2 V as shown in figure 5a at room temperature.

Figure 5a shows the charge/discharge profile of Li/C-$LiFePO_4$ half-cells for the first and fifteenth cycles. Independently of the cycle number, the typical flat voltage plateau at around 3.4 is observed, indicating the presence of a two-phase Fe^{2+}/Fe^{3+} redox reaction between $FePO_4$ and $LiFePO_4$ [57]. The first charge and discharge cycle show a capacity of 51.2 $mAh.g^{-1}$ and 50.5 $mAh.g^{-1}$, respectively (figure 5a). This relatively low charge/discharge capacity is related to the low ionic conductivity of the sample.

Figure 5a shows the good agreement between the theoretical simulations (blue line) and the experimental results for this scan rate, the small differences between the curves being attributed to the differences in the diffusion coefficient value assumed in the theoretical model.

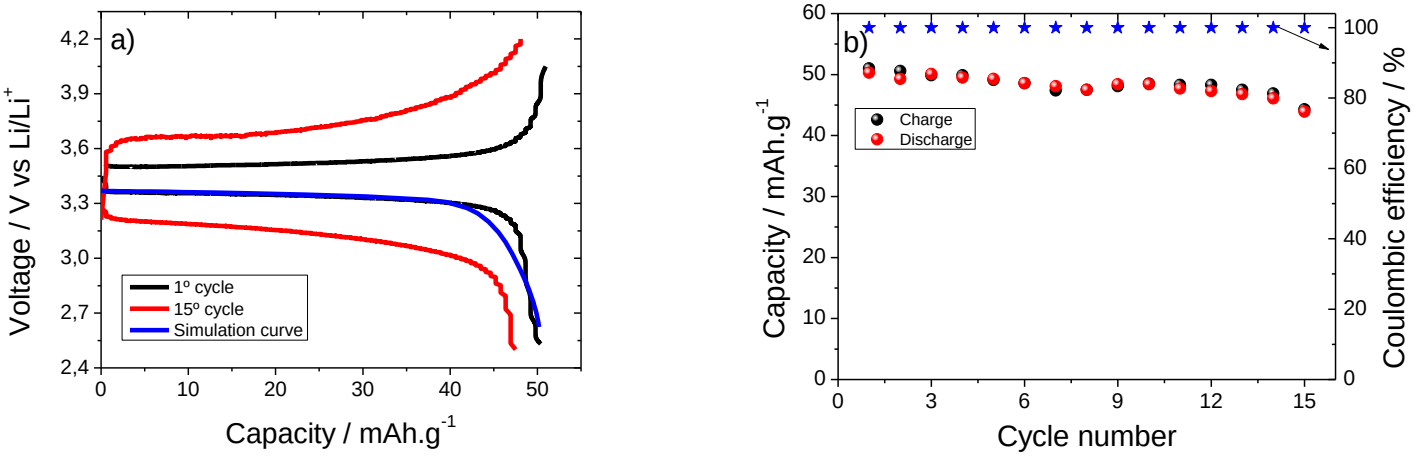

Figure 5 - 1st and 15th charge and discharge room temperature cycles at C/20 rate and theoretical simulation curve (a). Charge and discharge capacity and coulombic efficiency as a function of cycle number (b).

Figure 5b shows the charge/discharge specific capacity as a function of cycle number at C/20. The charge and discharge capacity are 43.9 $mAh.g^{-1}$ and 43.7 $mAh.g^{-1}$, respectively, in the 15 cycle and the coulombic efficiency is about 99%. It is observed that capacity fade is low and the excellent coulombic efficiency value indicates good reversibility of the process independently of the number of cycles.

It is an increasing effort in developing SPEs such as, P(VDF−HFP)/PVAc with $BaTiO_3$ [58], $P(EO)_1(LiTFSI)_{0.1}(PYR_{14}TFSI)_{0.1}$ [59] and polymeric ionic liquid [60], but the

charge-discharge tests are typically reported at 40 ºC and 80 ºC, respectively. The main advantage of our results when compared with the literature is the charge-discharge behavior at room temperature.

4.3.2. Theoretical simulation results

In order to understand battery performance and thus to be able to further optimize it, theoretical simulations have been carried out. The solid-state battery used in the theoretical simulations presents the same characteristics obtained in the experimental cyclic behavior (figure 5a) with 80% lithium concentration, 20% free ions in the solid polymer electrolyte and thickness of 100 μm. The lithium concentration in the solid polymer electrolyte was calculated considering the LiTFSI weight added to the PVDF-HFP polymer. Figure 5a shows the good agreement between experimental and theoretical curves, allowing the validation of the theoretical model for solid state batteries

Figure 6a shows the simulated discharge profile of this sample at different C-rates.

It is observed that the discharge capacity value and voltage plateau decrease with increasing C-rate due to the migration of the lithium ion and solid lithium species, resulting in higher internal losses for higher currents. This fact can be explained by the solid lithium concentration in which, when a maximum value is obtained, the discharge voltage reduces rapidly [34]. Figure 6a also shows that the maximum operating rate of the solid-state battery is C/2.

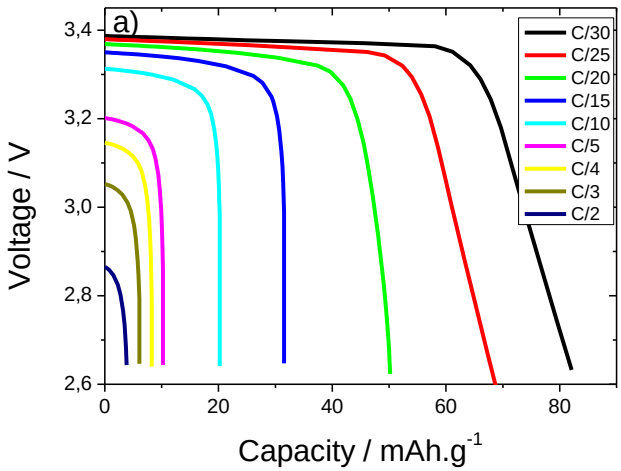

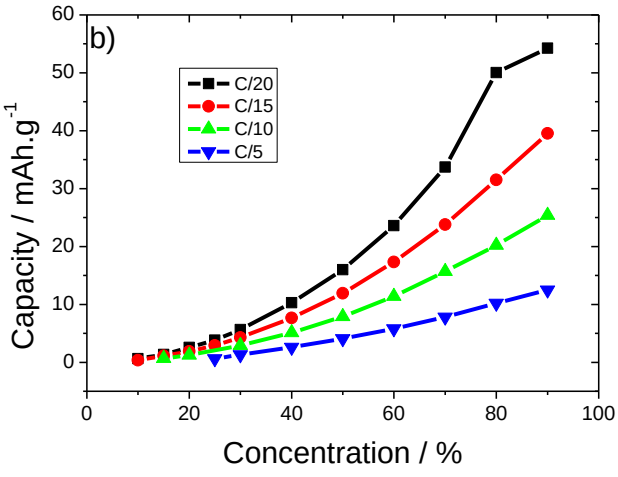

Figure 6 – Discharge profiles at different scan rates between C/30 to C/2 for PVDF-HFP/LiTFSI composites with thickness of 100 μm (a) and discharge value at different C-rates as a function of lithium concentration (b).

Figure 6b shows the discharge capacity as a function of lithium concentration between 10 to 90% at different C-rates (C/20, C/15, C/10, C/5) from solid electrolytes with a thickness of 100 μm and 20% of free ions. Regardless of C-rate, it is observed that the discharge capacity value increases with increasing lithium concentration, which is also related to increased diffusion rate allowing Li-ions to more freely travel through the electrolyte. In addition, it is noted that, depending on the C-rate applied to the solid-state battery, there is a minimum lithium concentration to operate the battery.

For the C/20 and C/15 rates, the battery do not operate below of 10% of lithium concentration but for C/10 and C/5, the minimum lithium concentration is 15% and 25%, respectively. The reason for this fact is due to the solid Li diffusion which is most significant for high discharge current.

The influence of solid polymer electrolyte thickness on battery performance at different C-rates (C/20, C/10 and C/5) was studied for 80% lithium concentration and 20% free ions as shown in figure 7.

Figure 7a-b shows the discharge capacity value as a function of solid polymer electrolyte thickness between 25 μm to 300 μm for C/20 and C/5, respectively.

For these C-rates (figure 7a-b) it is observed that the discharge capacity value is nearly independent of the thickness of the solid polymer electrolyte. This fact is observed in more detail in figure 7c, representing the discharge capacity as a function of solid polymer electrolyte thickness, which is constant for C/10 and C/5 rates. For the C/20 rate, the discharge capacity value decreases with increasing thickness due to the slower Li-ion motion towards the positive electrode. At the electrolyte/electrode interface Li-ion motion is reduced becoming solid lithium which diffuse through the positive electrode to allow further reactions at the interface [34].

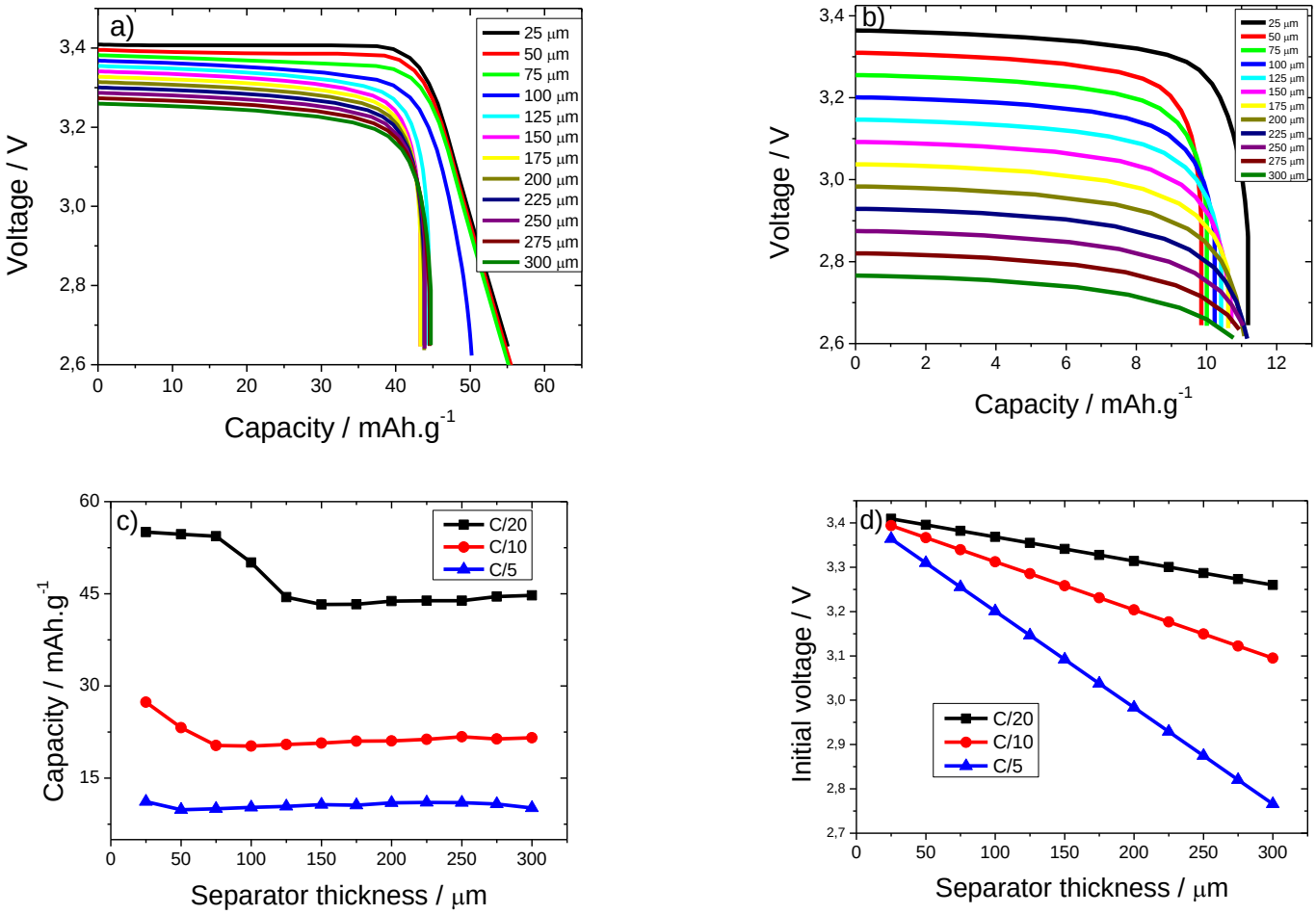

Figure 7 – Discharge profiles for different sample thickness at C/20 (a) and C/5 (b) for PVDF-HFP/LiTFSI composite with 80 wt.% of LITFSI. Discharge capacity value (c) and initial voltage value (d) as a function of sample thickness for C/20, C/10 and C/5 rates.

Figure 7d shows that for all C-rates the voltage plateau decreases with increasing electrolyte thickness due to concentration variations in the solid polymer electrolyte and in the positive electrode. Those variations are due to the voltage plateau of the equilibrium potential towards the end of the discharge, compared to the large initial equilibrium voltage drop for a fully charged battery [34, 35].

Both dissociation and recombination rates (k_{diss} and k_{rec}) are linked via the fraction of free lithium ions, δ (see equation in Table 1). Figure 8 shows the discharge capacity value as a function of the fraction of free lithium ions for different lithium concentration at C/20 and solid polymer electrolyte thickness of 100 µm.

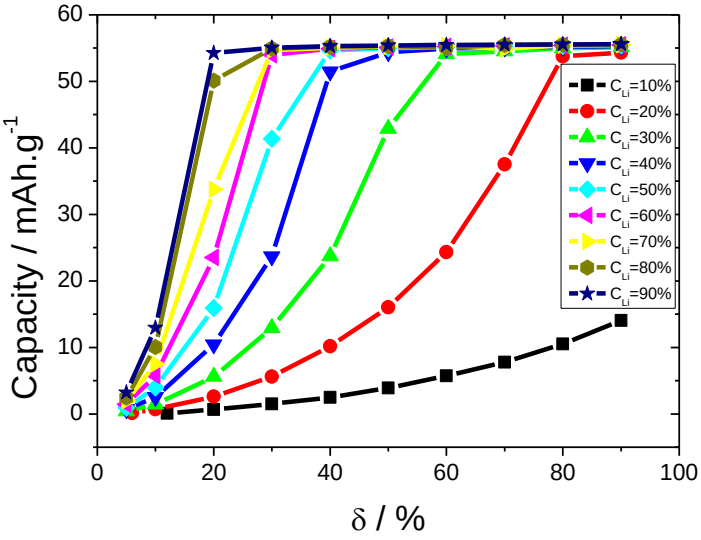

Figure 8 – Discharge capacity value as a function of percentage of free ions within the sample for different lithium ion concentrations at C/20 rate.

For lithium concentrations between 10% and 90%, the percentage of free ions in the solid polymer electrolyte varies between 5% and 90%, as it is shown in figure 8.

Regardless of the lithium concentration, it is observed that the discharge capacity value increases with increasing the percentage of free ions. Increasing the percentage of free ions in the solid polymer electrolyte allows increasing the rate of dissociation / recombination of the ions in the solid polymer electrolyte, which leads to higher battery performance. Further, the presence of high amounts of free ions in the solid polymer electrolyte facilitates the mobility and diffusion thereof, thus obtaining a consequent reduction of the resistance to this mobility. The simulated results quantify how solid polymer electrolyte performance can be tailored by the lithium concentration and percentage of free ions to improve the solid-state battery performance.

5. Conclusions

Solid polymer electrolytes (SPE) based on poly(vinylidene fluoride-co-hexafluoropropylene), PVDF-HFP, copolymer and lithium bis(trifluoromethanesulfonyl)imide (LiTFSI) have been prepared by solvent casting and the effect of LiTFSI content on ionic conductivity and other physical properties evaluated.

PVDF-HFP/LiTFSI composites show a porous morphology. Their thermal and mechanical properties correlate with the LiTFSI content. Incorporation of LiTFSI into PVDF-HFP decreases the melting enthalpy and thermal stability of the polymer as well as the Young's modulus when compared with pristine PVDF-HFP pristine. Further, FTIR demonstrated the ion-polymer interaction.

The ionic conductivity of the PVDF-HFP/LiTFSI composites increases with LiTFSI content in the composites, the best ionic conductivity of 0.0011 mS/cm at 25º C and 0.23 mS/cm at 90 ºC being obtained for PVDF-HFP/LiTFSI composites with 80wt.% LiTFSI content.

The electrochemical performance of the Li/C-$LiFePO_4$ half-cells at room temperature with this composite leads a discharge capacity of 51.2 $mAh.g^{-1}$ at C/20.

The theoretical simulation of the solid-state lithium-ion battery allows obtaining a correlation between cycling performance and lithium concentration, percentage of free ions and solid polymer electrolyte thickness. The theoretical results allow designing and improving battery performance by lithium concentration and percentage of free ions. The solid polymer electrolyte thickness does not affect the discharge capacity value, but the voltage plateau.

Thus, the developed solid polymer electrolyte represents a step forward towards the next generation of safer solid-state Li-ion batteries.

Nomenclature

List of symbols	
c_{Li^+}	concentration of lithium-ions, mol/m^3
c_{0,Li^+}	initial concentration of lithium-ions, mol/m^3
c_{Li}	solid lithium concentration, mol/m^3

$c_{Li,max}$	maximal lithium activity in the positive electrode, mol/m^3
$c_{Li,min}$	minimum lithium concentration in the positive electrode, mol/m^3
c_{n^-}	concentration of negative ions, mol/m^3
D_i	diffusion coefficient for species i (i=Li^+, n^-), m^2/s
D_{Li}	diffusion coefficient of solid lithium through the electrolyte at positive electrode, m^2/s
$E_{eq,i}$	equilibrium potential in the electrode (i=c), V
F	Faraday's constant, 96487 C/mol
i_{neg}	current density at negative electrode, A/m^2
i_c	current density at positive electrode, A/m^2
$i_{0,c}$	initial current density at positive electrode, A/m^2
i_{app}	applied current density at 1C, A/m^2
k_{diss}	dissociation reaction rate, 1/s
k_{rec}	recombination reaction rate, m^3/mol.s
k_{neg}	charge transfer reaction rate constant at negative electrode, mol/m^2.s^{-1}
k_c	charge transfer reaction rate constant at positive electrode, mol/m^2.s^{-1}
L_i	width of the battery component (*i=sep,c*) , m
N_i	transport value of species i (i=Li), mol/m^2
R	gas constant, 8,314 J/mol K
r_{Li^+}	lithium ion recombination/dissociation rate, mol/m^3.s
T	temperature, K
t	time, s
z_i	charge of species i *(i=Li^+, n^-)*
	Greek symbols
α_{neg}	charge transfer coefficient at negative electrode
α_c	charge transfer coefficient at positive electrode
δ	fraction of free lithium ions in equilibrium
ϕ_0	electric potential initial value, V

ϕ_E	electrolyte potential, V
η	over-potential, V
Subscripts referring specific components of the battery and initial condition	
c	cathode
neg	negative electrode
sep	separator
0	initial condition

Acknowledgments

The authors thank the FCT (Fundação para a Ciência e Tecnologia) for financial support under the framework of Strategic Funding grants UID/FIS/04650/2013, UID/EEA/04436/2013 and UID/QUI/0686/2016; and project no. PTDC/FIS-MAC/28157/2017. The authors also thank the FCT for financial support under grant SFRH/BPD/112547/2015 (C.M.C.). Financial support from the Basque Government Industry Department under the ELKARTEK and HAZITEK programs is also acknowledged. JMMD and JLGR acknowledge funding by the Spanish Ministry of Economy and Competitiveness (MINECO) through the project MAT2016-76039-C4-1 and 3-R (including the FEDER financial support) CIBER-BBN is an initiative funded by the VI National R&D&i Plan 2008–2011, Iniciativa Ingenio 2010, Consolider Program, CIBER Actions and financed by the Instituto de Salud Carlos III with assistance from the European Regional Development Fund.

References

[1] X. Lin, M. Salari, L.M.R. Arava, P.M. Ajayan, M.W. Grinstaff, High temperature electrical energy storage: advances, challenges, and frontiers, Chemical Society Reviews 45(21) (2016) 5848-5887.DOI: 10.1039/C6CS00012F.

[2] A. Manthiram, An Outlook on Lithium Ion Battery Technology, ACS Central Science 3(10) (2017) 1063-1069.DOI: 10.1021/acscentsci.7b00288.

[3] G.E. Blomgren, The Development and Future of Lithium Ion Batteries, Journal of The Electrochemical Society 164(1) (2017) A5019-A5025.DOI: 10.1149/2.0251701jes.

[4] A. Kraytsberg, Y. Ein-Eli, Higher, Stronger, Better… A Review of 5 Volt Cathode Materials for Advanced Lithium-Ion Batteries, Advanced Energy Materials 2(8) (2012) 922-939.DOI: doi:10.1002/aenm.201200068.

[5] H. Lee, M. Yanilmaz, O. Toprakci, K. Fu, X. Zhang, A review of recent developments in membrane separators for rechargeable lithium-ion batteries, Energy & Environmental Science 7(12) (2014) 3857-3886.DOI: 10.1039/C4EE01432D.

[6] M.A. Navarra, J. Manzi, L. Lombardo, S. Panero, B. Scrosati, Ionic Liquid-Based Membranes as Electrolytes for Advanced Lithium Polymer Batteries, ChemSusChem 4(1) (2011) 125-130.DOI: doi:10.1002/cssc.201000254.

[7] D. Aurbach, A. Schechter, Advanced Liquid Electrolyte Solutions, in: G.-A. Nazri, G. Pistoia (Eds.), Lithium Batteries: Science and Technology, Springer US, Boston, MA, 2003, pp. 530-573.

[8] Y. Liu, Q. Liu, L. Xin, Y. Liu, F. Yang, E.A. Stach, J. Xie, Making Li-metal electrodes rechargeable by controlling the dendrite growth direction, Nature Energy 2 (2017) 17083.DOI: 10.1038/nenergy.2017.83
https://www.nature.com/articles/nenergy201783#supplementary-information.

[9] W.H. Meyer, Polymer Electrolytes for Lithium-Ion Batteries, Advanced Materials 10(6) (1998) 439-448.DOI: doi:10.1002/(SICI)1521-4095(199804)10:6<439::AID-ADMA439>3.0.CO;2-I.

[10] C. Sun, J. Liu, Y. Gong, D.P. Wilkinson, J. Zhang, Recent advances in all-solid-state rechargeable lithium batteries, Nano Energy 33 (2017) 363-386.DOI: https://doi.org/10.1016/j.nanoen.2017.01.028.

[11] P.V. Wright, Polymer electrolytes—the early days, Electrochimica Acta 43(10) (1998) 1137-1143.DOI: https://doi.org/10.1016/S0013-4686(97)10011-1.

[12] J. Nunes-Pereira, C.M. Costa, S. Lanceros-Méndez, Polymer composites and blends for battery separators: State of the art, challenges and future trends, Journal of Power Sources 281 (2015) 378-398.DOI: https://doi.org/10.1016/j.jpowsour.2015.02.010.

[13] J. Barbosa, J. Dias, S. Lanceros-Méndez, C. Costa, Recent Advances in Poly(vinylidene fluoride) and Its Copolymers for Lithium-Ion Battery Separators, Membranes 8(3) (2018) 45.

[14] C.M. Costa, M.M. Silva, S. Lanceros-Méndez, Battery separators based on vinylidene fluoride (VDF) polymers and copolymers for lithium ion battery applications, RSC Advances 3(29) (2013) 11404-11417.DOI: 10.1039/C3RA40732B.

[15] A.M. Elmér, P. Jannasch, Polymer electrolyte membranes by in situ polymerization of poly(ethylene carbonate-co-ethylene oxide) macromonomers in blends with poly(vinylidene fluoride-co-hexafluoropropylene), Journal of Polymer Science Part B: Polymer Physics 45(1) (2007) 79-90.DOI: doi:10.1002/polb.20980.

[16] W. Gorecki, M. Jeannin, E. Belorizky, C. Roux, M. Armand, Physical properties of solid polymer electrolyte PEO(LiTFSI) complexes, Journal of Physics: Condensed Matter 7(34) (1995) 6823.

[17] H.J. Alcock, O.C. White, G. Jegelevicius, M.R. Roberts, J.R. Owen, New high-throughput methods of investigating polymer electrolytes, Journal of Power Sources 196(6) (2011) 3355-3359.DOI: https://doi.org/10.1016/j.jpowsour.2010.11.098.

[18] J. Bai, H. Lu, Y. Cao, X. Li, J. Wang, A novel ionic liquid polymer electrolyte for quasi-solid state lithium air batteries, RSC Advances 7(49) (2017) 30603-30609.DOI: 10.1039/C7RA05035F.

[19] S. Ferrari, E. Quartarone, P. Mustarelli, A. Magistris, M. Fagnoni, S. Protti, C. Gerbaldi, A. Spinella, Lithium ion conducting PVdF-HFP composite gel electrolytes based on N-methoxyethyl-N-methylpyrrolidinium bis(trifluoromethanesulfonyl)-imide ionic liquid, Journal of Power Sources 195(2) (2010) 559-566.DOI: https://doi.org/10.1016/j.jpowsour.2009.08.015.

[20] Nojan Aliahmad, Sudhir Shrestha, Kody Varahramyan, M. Agarwal, Poly(vinylidene fluoride-hexafluoropropylene) polymer electrolyte for paper-based and flexible battery applications, AIP Advances 6(6) (2016) 065206.DOI: 10.1063/1.4953811.

[21] S. Suriyakumar, M. Kanagaraj, N. Angulakshmi, M. Kathiresan, K.S. Nahm, M. Walkowiak, K. Wasiński, P. Półrolniczak, A.M. Stephan, Charge–discharge studies of all-solid-state Li/LiFePO4 cells with PEO-based composite electrolytes encompassing metal organic frameworks, RSC Advances 6(99) (2016) 97180-97186.DOI: 10.1039/C6RA17962B.

[22] A. Zalewska, J. Dumińska, N. Langwald, J. Syzdek, M. Zawadzki, Preparation and performance of gel polymer electrolytes doped with ionic liquids and surface-modified inorganic fillers, Electrochimica Acta 121 (2014) 337-344.DOI: https://doi.org/10.1016/j.electacta.2013.12.135.

[23] H. Ye, J. Huang, J.J. Xu, A. Khalfan, S.G. Greenbaum, Li Ion Conducting Polymer Gel Electrolytes Based on Ionic Liquid/PVDF-HFP Blends, Journal of The Electrochemical Society 154(11) (2007) A1048-A1057.DOI: 10.1149/1.2779962.

[24] W. Zhang, J. Nie, F. Li, Z.L. Wang, C. Sun, A durable and safe solid-state lithium battery with a hybrid electrolyte membrane, Nano Energy 45 (2018) 413-419.DOI: https://doi.org/10.1016/j.nanoen.2018.01.028.

[25] X. Ban, W. Zhang, N. Chen, C. Sun, A High-Performance and Durable Poly(ethylene oxide)-Based Composite Solid Electrolyte for All Solid-State Lithium Battery, The Journal of Physical Chemistry C 122(18) (2018) 9852-9858.DOI: 10.1021/acs.jpcc.8b02556.

[26] Y. Zhang, J. Lai, Y. Gong, Y. Hu, J. Liu, C. Sun, Z.L. Wang, A Safe High-Performance All-Solid-State Lithium–Vanadium Battery with a Freestanding V2O5 Nanowire Composite Paper Cathode, ACS Applied Materials & Interfaces 8(50) (2016) 34309-34316.DOI: 10.1021/acsami.6b10358.

[27] H. Hou, Q. Xu, Y. Pang, L. Li, J. Wang, C. Zhang, C. Sun, Efficient Storing Energy Harvested by Triboelectric Nanogenerators Using a Safe and Durable All-Solid-State Sodium-Ion Battery, Advanced Science 4(8) (2017) 1700072.DOI: doi:10.1002/advs.201700072.

[28] J. Wang, C.-W. Sun, Y.-D. Gong, H.-R. Zhang, J.A. Alonso, M.T. Fernández-Díaz, Z.-L. Wang, J.B. Goodenough, Imaging the diffusion pathway of Al3+ ion in NASICON-type (Al0.2Zr0.8)20/19Nb(PO4)3 as electrolyte for rechargeable solid-state Al batteries, Chinese Physics B 27(12) (2018) 128201.DOI: 10.1088/1674-1056/27/12/128201.

[29] C.T. Imrie, M.D. Ingram, G.S. McHattie, Ion Transport in Glassy Polymer Electrolytes, The Journal of Physical Chemistry B 103(20) (1999) 4132-4138.DOI: 10.1021/jp983968e.

[30] C. Tao, M.-H. Gao, B.-H. Yin, B. Li, Y.-P. Huang, G. Xu, J.-J. Bao, A promising TPU/PEO blend polymer electrolyte for all-solid-state lithium ion batteries, Electrochimica Acta 257 (2017) 31-39.DOI: https://doi.org/10.1016/j.electacta.2017.10.037.

[31] C. Ribeiro, C.M. Costa, D.M. Correia, J. Nunes-Pereira, J. Oliveira, P. Martins, R. Gonçalves, V.F. Cardoso, S. Lanceros-Méndez, Electroactive poly(vinylidene fluoride)-based structures for advanced applications, Nature Protocols 13 (2018) 681.DOI: 10.1038/nprot.2017.157

https://www.nature.com/articles/nprot.2017.157#supplementary-information.

[32] A. Gören, D. Cíntora-Juárez, P. Martins, S. Ferdov, M.M. Silva, J.L. Tirado, C.M. Costa, S. Lanceros-Méndez, Influence of Solvent Evaporation Rate in the Preparation of

Carbon-Coated Lithium Iron Phosphate Cathode Films on Battery Performance, Energy Technology 4(5) (2016) 573-582.DOI: doi:10.1002/ente.201500392.

[33] S. Li, Q. Wu, D. Zhang, Z. Liu, Y. He, Z.L. Wang, C. Sun, Effects of pulse charging on the performances of lithium-ion batteries, Nano Energy 56 (2019) 555-562.DOI: https://doi.org/10.1016/j.nanoen.2018.11.070.

[34] A. Bates, S. Mukherjee, N. Schuppert, B. Son, J.G. Kim, S. Park, Modeling and simulation of 2D lithium-ion solid state battery, International Journal of Energy Research 39(11) (2015) 1505-1518.DOI: doi:10.1002/er.3344.

[35] D. Danilov, R.A.H. Niessen, P.H.L. Notten, Modeling All-Solid-State Li-Ion Batteries, Journal of The Electrochemical Society 158(3) (2011) A215-A222.DOI: 10.1149/1.3521414.

[36] S.D. Fabre, D. Guy-Bouyssou, P. Bouillon, F. Le Cras, C. Delacourt, Charge/Discharge Simulation of an All-Solid-State Thin-Film Battery Using a One-Dimensional Model, Journal of The Electrochemical Society 159(2) (2011) A104-A115.DOI: 10.1149/2.041202jes.

[37] P. Martins, A.C. Lopes, S. Lanceros-Mendez, Electroactive phases of poly(vinylidene fluoride): Determination, processing and applications, Progress in Polymer Science 39(4) (2014) 683-706.DOI: https://doi.org/10.1016/j.progpolymsci.2013.07.006.

[38] A. Munch Elmér, P. Jannasch, Gel electrolyte membranes derived from co-continuous polymer blends, Polymer 46(19) (2005) 7896-7908.DOI: https://doi.org/10.1016/j.polymer.2005.06.079.

[39] M. Ulaganathan, C.M. Mathew, S. Rajendran, Highly porous lithium-ion conducting solvent-free poly(vinylidene fluoride-co-hexafluoropropylene)/poly(ethyl methacrylate) based polymer blend electrolytes for Li battery applications, Electrochimica Acta 93 (2013) 230-235.DOI: https://doi.org/10.1016/j.electacta.2013.01.100.

[40] R.E. Sousa, J. Nunes-Pereira, J.C.C. Ferreira, C.M. Costa, A.V. Machado, M.M. Silva, S. Lanceros-Mendez, Microstructural variations of poly(vinylidene fluoride co-hexafluoropropylene) and their influence on the thermal, dielectric and piezoelectric properties, Polymer Testing 40 (2014) 245-255.DOI: https://doi.org/10.1016/j.polymertesting.2014.09.012.

[41] S. Jeschke, M. Mutke, Z. Jiang, B. Alt, H.-D. Wiemhöfer, Study of Carbamate-Modified Disiloxane in Porous PVDF-HFP Membranes: New Electrolytes/Separators

for Lithium-Ion Batteries, ChemPhysChem 15(9) (2014) 1761-1771.DOI: doi:10.1002/cphc.201400065.

[42] W. Kam, C.-W. Liew, J.Y. Lim, S. Ramesh, Electrical, structural, and thermal studies of antimony trioxide-doped poly(acrylic acid)-based composite polymer electrolytes, Ionics 20(5) (2014) 665-674.DOI: 10.1007/s11581-013-1012-0.

[43] J. Amici, M. Alidoost, C. Francia, S. Bodoardo, S. Martinez Crespiera, D. Amantia, M. Biasizzo, F. Caldera, F. Trotta, O2 selective membranes based on a dextrin-nanosponge (NS) in a PVDF-HFP polymer matrix for Li–air cells, Chemical Communications 52(94) (2016) 13683-13686.DOI: 10.1039/C6CC06954A.

[44] Shalu, L. Balo, H. Gupta, V.k. Singh, R.K. Singh, Mixed anion effect on the ionic transport behavior, complexation and various physicochemical properties of ionic liquid based polymer gel electrolyte membranes, RSC Advances 6(77) (2016) 73028-73039.DOI: 10.1039/C6RA10340E.

[45] C.L. Cheng, C.C. Wan, Y.Y. Wang, Preparation of porous, chemically cross-linked, PVdF-based gel polymer electrolytes for rechargeable lithium batteries, Journal of Power Sources 134(2) (2004) 202-210.DOI: https://doi.org/10.1016/j.jpowsour.2004.03.037.

[46] K.P. Menard, Dynamic Mechanical Analysis: A Practical Introduction, Second Edition, CRC Press2008.

[47] B.-Y. Chang, S.-M. Park, Electrochemical Impedance Spectroscopy, Annual Review of Analytical Chemistry 3(1) (2010) 207-229.DOI: 10.1146/annurev.anchem.012809.102211.

[48] S.-M. Park, J.-S. Yoo, Peer Reviewed: Electrochemical Impedance Spectroscopy for Better Electrochemical Measurements, Analytical Chemistry 75(21) (2003) 455 A-461 A.DOI: 10.1021/ac0313973.

[49] F.M. Gray, Solid Polymer Electrolytes: Fundamentals and Technological Applications, Wiley1991.

[50] R.D. Armstrong, T. Dickinson, P.M. Willis, The A.C. impedance of powdered and sintered solid ionic conductors, Journal of Electroanalytical Chemistry and Interfacial Electrochemistry 53(3) (1974) 389-405.DOI: https://doi.org/10.1016/S0022-0728(74)80077-X.

[51] D.M. Correia, C.M. Costa, J. Nunes-Pereira, M.M. Silva, G. Botelho, J.L.G. Ribelles, S. Lanceros-Méndez, Physicochemical properties of poly(vinylidene fluoride-trifluoroethylene)/poly(ethylene oxide) blend membranes for lithium ion battery

applications: Influence of poly(ethylene oxide) molecular weight, Solid State Ionics 268 (2014) 54-67.DOI: https://doi.org/10.1016/j.ssi.2014.09.029.

[52] X. Li, Z. Wang, H. Lin, Y. Liu, Y. Min, F. Pan, Composite electrolytes of pyrrolidone-derivatives-PEO enable to enhance performance of all solid state lithium-ion batteries, Electrochimica Acta 293 (2019) 25-29.DOI: https://doi.org/10.1016/j.electacta.2018.10.023.

[53] J.-H. Baik, D.-G. Kim, J. Shim, J.H. Lee, Y.-S. Choi, J.-C. Lee, Solid polymer electrolytes containing poly(ethylene glycol) and renewable cardanol moieties for all-solid-state rechargeable lithium batteries, Polymer 99 (2016) 704-712.DOI: https://doi.org/10.1016/j.polymer.2016.07.058.

[54] H. Zeng, X. Ji, F. Tsai, Q. Zhang, T. Jiang, R.K.Y. Li, H. Shi, S. Luan, D. Shi, Enhanced cycling performance for all-solid-state lithium ion battery with LiFePO4 composite cathode encapsulated by poly (ethylene glycol) (PEG) based polymer electrolyte, Solid State Ionics 320 (2018) 92-99.DOI: https://doi.org/10.1016/j.ssi.2018.02.040.

[55] C. Li, H. Yue, Q. Wang, J. Li, J. Zhang, H. Dong, Y. Yin, S. Yang, A novel composite solid polymer electrolyte based on copolymer P(LA-co-TMC) for all-solid-state lithium ionic batteries, Solid State Ionics 321 (2018) 8-14.DOI: https://doi.org/10.1016/j.ssi.2018.03.031.

[56] J. Bao, X. Qu, G. Qi, Q. Huang, S. Wu, C. Tao, M. Gao, C. Chen, Solid electrolyte based on waterborne polyurethane and poly(ethylene oxide) blend polymer for all-solid-state lithium ion batteries, Solid State Ionics 320 (2018) 55-63.DOI: https://doi.org/10.1016/j.ssi.2018.02.030.

[57] Y.-H. Nien, J.R. Carey, J.-S. Chen, Physical and electrochemical properties of LiFePO4/C composite cathode prepared from various polymer-containing precursors, Journal of Power Sources 193(2) (2009) 822-827.DOI: https://doi.org/10.1016/j.jpowsour.2009.04.013.

[58] M. Sasikumar, M. Raja, R.H. Krishna, A. Jagadeesan, P. Sivakumar, S. Rajendran, Influence of Hydrothermally Synthesized Cubic-Structured BaTiO3 Ceramic Fillers on Ionic Conductivity, Mechanical Integrity, and Thermal Behavior of P(VDF–HFP)/PVAc-Based Composite Solid Polymer Electrolytes for Lithium-Ion Batteries, The Journal of Physical Chemistry C 122(45) (2018) 25741-25752.DOI: 10.1021/acs.jpcc.8b03952.

[59] G.-T. Kim, S. Passerini, M. Carewska, G. Appetecchi, Ionic Liquid-Based Electrolyte Membranes for Medium-High Temperature Lithium Polymer Batteries, Membranes 8(3) (2018) 41.
[60] K. Yang, Z. Liao, Z. Zhang, L. Yang, S.-i. Hirano, Ionic plastic crystal-polymeric ionic liquid solid-state electrolytes with high ionic conductivity for lithium ion batteries, Materials Letters 236 (2019) 554-557.DOI: https://doi.org/10.1016/j.matlet.2018.11.003.